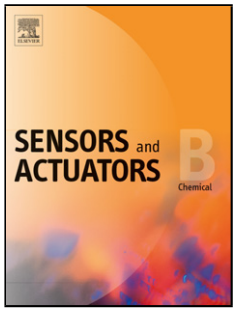

Title: One-step selective wettability modification of PMMA microfluidic devices by using controllable gradient UV irradiation (CGUI)

Authors: Chao Liang, Yuanchang Liu, Chong Liu, Xia Li, Li Chen, Chunzheng Duan, Jingmin Li

PII: S0925-4005(18)31271-1
DOI: https://doi.org/10.1016/j.snb.2018.07.034
Reference: SNB 25003

To appear in: *Sensors and Actuators B*

Received date: 10-4-2018
Revised date: 3-7-2018
Accepted date: 6-7-2018

Please cite this article as: Liang C, Liu Y, Liu C, Li X, Chen L, Duan C, Li J, One-step selective wettability modification of PMMA microfluidic devices by using controllable gradient UV irradiation (CGUI), *Sensors and Actuators: B. Chemical* (2018), https://doi.org/10.1016/j.snb.2018.07.034

One-step selective wettability modification of PMMA microfluidic devices by using controllable gradient UV irradiation (CGUI)

Chao Liang [a], Yuanchang Liu[c], Chong Liu [a, b,*], Xia Li[a], Li Chen[a], Chunzheng Duan[b], Jingmin Li[a*]

[a]Key Laboratory for Micro/Nano Technology and System of Liaoning Province, Dalian University of Technology, Dalian, China

[b]Key Laboratory for Precision and Non-traditional Machining Technology of Ministry of Education, Dalian University of Technology, Dalian, China

[c]Department of Mechanical Engineering, University College London, London, UK.

[*]**Corresponding Author:** E-mail: jingminl@dlut.edu.cn; chongl@dlut.edu.cn

Highlights

- A controllable gradient UV irradiation (CGUI) method for multi-regional selective modification of PMMA microfluidic device is demonstrated.
- A series of quartz plates sputtered with different thickness of Cu are used to adjust the UV irradiation transmitted to the PMMA surface.
- The –OH group and surface roughness of the PMMA surface are varied by using different Cu-sputtered quartz plates.
- The proposed method is applied to a fully integrated Point-of-Care Test device for the detection of cTnI achieving a low lower detection limit of 85pg/ml.

ABSTRACT:

Poly (methyl methacrylate) (PMMA) has become increasingly popular to fabricate microfluidic devices. In a microfluidic device, different functional areas usually require different wettability to achieve a better performance. However, most of the existing wettability modification methods have been applied to the whole PMMA surface making the device have minimum wettability difference. In this paper, a controllable gradient UV irradiation (CGUI) method was presented. In this method, a series of quartz plates sputtered with different thickness of Cu were arranged on top of the PMMA surface. By controlling the thickness of Cu film, the UV irradiation, which transmitted though the quartz plates onto the PMMA surface, can be adjusted making the modification performance able to be varied accordingly. The validation of the proposed CGUI was conducted through contact angle measurements. Our results showed that through 5mins CGUI process, the contact angle for different parts of the PMMA surface can be varied from 45.48° to 77.41° continuously with a long-term stability of 60 days. To demonstrate this method, a fully integrated Point-of-Care Test (POCT) device was designed and fabricated for the detection of cardiac Troponin I achieving the lower detection limit of 85pg/ml within 10mins.

Key words: selective wettability modification, polymer, UV/ozone, microfluidic device

1. Introduction

Compared with the inorganic materials, such as silicon and glass, which usually require the photolithography and etching technologies to fabricate the microfluidic networks [1, 2], polymer exhibits numerous advantages including the reduced cost, increased mechanical and optical properties, and ease of fabrication. Poly (methyl methacrylate) (PMMA), as a thermoplastic polymer, can be processed by hot embossing [3] and mold injecting [4], making it a commonly-used material for mass production. However, since the PMMA surface is nonpolar and thus has a low wettability [5, 6], the potential application of PMMA in the autonomous capillary microfluidic devices (ACMDs) has been limited. ACMDs, in which liquid can be driven by capillary force, attract extensive interest due to their features of portability, low dead volume and small power consumption and have been subsequently applied in various fields, such as medical diagnostics [7], environmental sampling [8] and pharmaceutical analysis [9].

The microchannel surface in the ACMDs should be hydrophilic to establish the spontaneous filling and to achieve this, a number of hydrophilic modification methods have been successfully developed with demonstrated capabilities. These methods can generally be classified into two categories. The first one is the high-energy treatment, such as the plasma treatment using different gases [10], the irradiation with ion beam [11], or the corona discharge [12]. With the implementation of these treatments, some hydroxyl groups can be introduced to the polymer surface and subsequently render the material hydrophilic. The second one is wet chemical treatment, which adopts the way of coating or grafting some polar functionalities onto the polymer surface. For example, poly (ethyleneglycol) was grafted onto the PMMA surfaces of capillary electrophoresis microchips to make the surface hydrophilic [13]. Also, a nano-colloidal TiO_2 sol was reported to be coated onto a polymer surface for its hydrophilic modification, which was performed to generate an emulsion in a microfluidic system [14]. While these treatments can be used to change the surface wettability, some of the modified surface can undergo hydrophobic recovery within a couple of hours [15] and other issues such as microchannel contamination or involving multiple and complicated steps, also exist. At the same time, in a fully integrated ACMD, different flow rates such as slow rate for incubation, medium rate for reaction and fast rate for

washing are usually required to achieve better application performance and more function integrations in one microchannel,. Nevertheless, all of these hydrophilic treatments were performed to the whole polymer surface, which cannot direct the desired wettability to the specific sites in the microchannel. Given that the microfluidic flow is predominately influenced by the sample properties, microchannel surface wettability and channel geometry, to tune the flow rate, some microstructures have to be fabricated in the microchannel. Some microstructures of various shapes, which were named as capillary pumps, were positioned into the microchannel to generate the flow rate differences [16]. Researchers reported some valve structures in the ACMDs, which utilize an abruptly changing geometry of the flow path to delay or even stop a moving liquid filling front in a microchannel [17]. However, the aforementioned structures were all very complicated, which required the cumbersome microfabrication techniques.

UV/ ozone generated from a low-pressure mercury lamp was first applied to remove the photoresist polymers from the substrate [18] and then it was used to decrease the glass transition temperature of the polymer and achieve the low temperature thermal bonding of the microfluidic devices [19]. Recently, researchers utilized the UV/ ozone to enhance the adhesion between metal films and polymer substrates [20]. In fact, UV/ ozone treatment was also a commonly-used method of hydrophilic treatment for the polymer surface. However, in previous researches, the whole polymer surface was taken under the UV/ ozone treatment leaving no wettability-gradient [21]. Or else, only one-gradient was induced by covering part of the surface with opaque masks, which completely blocked the UV irradiation [22]. To the best of our knowledge, it is the first time to achieve a one-step selective wettability modification of PMMA microfluidic devices by using controllable gradient UV irradiation.

In this paper, a controllable gradient UV irradiation (CGUI) method to render the PMMA surface selective wettability was developed and demonstrated. In this method, a series of quartz plates, which were sputtered with different thickness of Cu, were first arranged on top of the PMMA surface and then submitted to the UV/ozone irradiation. By controlling the thickness of Cu film, the UV irradiation, which transmitted though the quartz plates onto the PMMA surface, can be adjusted and subsequently achieve the wettability-gradient modification performance. To reveal such a variation in the

performance, UV-visible spectrophotometer has been used to evaluate the relationship between the Cu film thickness and the UV irradiation. To further provide an insight into the CGUI method, analysis of the attenuated total reflection Fourier-transform infrared spectrometry (ATR-FTIR) and surface morphology for the modified surface has also been conducted. By implementing the proposed CGUI method, two different types of ACMDs with the straight and serpentine microchannel respectively, were first fabricated to testify the flow behavior. Then, a fully integrated Point-of-Care Test (POCT) device completely driven by capillary force was designed and fabricated to detect cardiac Troponin I (cTnI), which is considered to be one of the gold standard biomarkers for the diagnosis of acute myocardial infarction. Our results showed that through 5mins CGUI process, a continuous variation in contact angle of the PMMA surface from 45.48° to 77.41° can be achieved with a long-term stability of 60 days. Such a wettability variation is capable of generating differential flow rate without changing the microchannel geometry, which makes the processes of the priming, time-delaying and emptying proceed automatically. The lower detection limit of 85pg/ml for cTnI was obtained within 10 mins. Considering that the clinically applicable concentration was 0.01–0.1 ng/ml [23, 24], this method has the potential to be used in the clinical applications. It can be expected that by applying the CGUI method a new generation ACMD with the feature of "smart" wettability control can be achieved.

2. Principle: capillary flow in the microchannel

In an ACMD, the liquid in the microchannel is driven by the capillary force. The flow rate is determined by the surface wettability of the ACMD, the viscosity of the liquid, the flow resistance and the capillary pressure, which can be calculated by:

$$Q = \frac{1}{\eta}\frac{\Delta P}{R_F} \tag{1}$$

where η is the viscosity of the liquid, ΔP is the difference in pressure inside and in front of the liquid, which can be taken as the capillary pressure P_C in the ACMD, and R_F is the flow resistance along the flow path. P_C within the channel can be obtained from the subsequent equation [25].

$$P_c = -\gamma\left[\left(\frac{\cos\alpha_t + \cos\alpha_b}{h}\right) + \left(\frac{\cos\alpha_l + \cos\alpha_r}{w}\right)\right] \tag{2}$$

where γ is the surface tension of the liquid, and α_t, α_b, α_l, α_r are the contact angles of the top, bottom, left and right walls for the channel. The flow resistance R_F can be calculated by [13]

$$R_F = \left[\frac{1}{12}\left(1+\frac{5}{6}\frac{h}{w}\right)\frac{hwR_H^2}{L}\right]^{-1} \tag{3}$$

where h is the depth of the microchannel, w is the width, L is the length and R_H is the hydraulic radius of the microchannel, which can be calculated as the ratio of the cross sectional area by half the wetted perimeter

$$R_H = \frac{A}{P/2} = \frac{h\,w}{h+w} \tag{4}$$

The flow rate can be estimated by the capillary pressure divided by the flow resistance. From the above theoretical analysis, it can be seen that by varying the wettability or geometry of the microchannel, the flow rate can be changed accordingly. Moreover, while the wettability and geometry of the microchannel remain the same, the flow rate will decrease as the liquid continuously fills the microchannel. That is because the flow resistance R_F will increase as the filling length increases. In the following section, we elucidate how to generate selective wettability on the same PMMA surface on the PMMA surface through one-step UV/ozone treatment and what the corresponding flow behavior is.

3. Experimental section

3.1 Design and fabrication of CGUI device

Fig. 1a illustrates the proposed CGUI method. A commercial-available UV/ozone cleaner (144AX-220, Jelight Co., Inc., USA) was used to perform the CGUI process. The UV/ozone cleaner was equipped with a low pressure mercury vapor grid with an output power of 28mW/cm^2 capable of emitting UV lights at 185 and 254 nm wavelengths with the maximum exposure area of 30×30cm^2. The oxygen molecules (O_2) in the UV/ozone chamber can absorb the 185 nm UV irradiation and form ozone (O_3). After that, the O_3 molecules can absorb the 254 nm UV light and turn into atomic oxygen (O).

A series of quartz plates, which were sputtered with different thickness of Cu, were arranged between the polymer

surface and the UV lamp. The quartz plates were purchased from Jinghe Company (Jiangsu, China) with the size being 1mm in thickness and the length and the width depending on the modification area. A sputtering system (LAB 18, Kurt J. Lesker Co., USA) with the power of 300W was applied to perform the sputtering process. The sputtering time was set to be 2s, 5s, 8s, 11s and 14s to generate different thickness of Cu film on five separate quartz plates. It should be noted that as the sputtering time exceeded 14s, the quartz plates became completely opaque. For the purpose of better illustration, the corresponding quartz plates were named mask B, C, D, E and F, respectively, while mask A indicates the plate with no Cu being sputtered. The thickness of the Cu film was measured using a white-light interferometer (New view5022, ZYGO, USA). The UV transmittance measurement of the five quartz plates was conducted using a UV-Vis spectrophotometer (Cary 300, Agilent Co., USA) with the emission wavelength ranging from 190nm to 400nm.

A CGUI device was designed and fabricated. The solid model of such a device is shown in Fig. 1b. It can be observed that the device mainly comprised of three parts, i.e. the quartz fixture, the microdevice fixture and the holder. An inserting slot has been designed to be included in the quartz fixture so that quartz plate with Cu film can be properly inserted. Also, at the end of the fixture, three springs were added to provide a clamping force, which is able to prevent light leakage from the clearance of the adjacent quartz plates. The sequence of the quartz plates can be arranged in the slots based on the application demands. The different wettability on the same surface can be generated according to the arrangements of the quartz plates. The holder contained several adjusting grooves, which provides a varying distance between the polymer surface and the UV lamp ranging from 2cm to 10cm. The components of the CGUI device were first cut from PMMA sheets using a CO_2 laser machining before being bolted together. Since the UV light cannot transmit through the PMMA material, it will not have an impact on the application performance.

3.2 Characterization of modified surface

To validate the CGUI performance, several 2mm thick PMMA sheets (Asahi, Kasei) were cut into 100×30mm and the quartz plates were first inserted into the inserting slot of the quartz fixture by a given sequence. Then, the PMMA sheets were placed into the microdevice fixture. Subsequently, the quartz fixture and the microdevice fixture were mounted

into the holder with a fixed distance of 5cm between the PMMA sheet and the UV lamp. After that, the device was placed into the UV/ozone chamber for CGUI. The modification time was set to be 1min, 3min, 5min, 7min and 9min. After each modification, the contact angle of the modified surface was measured using a drop shape analyzer (DAS 100, KRUSS Co., Germany). Each measurement was conducted three times on three individual PMMA sheets.

To obtain an insight into the modification mechanism, the attenuated total reflection Fourier-transform infrared spectrometry (ATR-FTIR) and surface morphology measurements for the modified surface were performed. The ATR-FTIR measurement was conducted by using a Vertex 70 FTIR with a Platinum ATR accessory equipped with a single reflection diamond crystal (Bruker, Germany), and the angle of incidence was 45°. The spectra were recorded from 4000 to 400 cm^{-1} by collecting 64 scans with the resolution of $2cm^{-1}$. The surface morphology was investigated using a white-light interferometer (New view5022, ZYGO, USA) with a 0.1nm resolution at the vertical direction.

3.3 Fabrication of the ACMDs for flow behavior validation

In order to validate the flow behaviours after using the CGUI method, two kinds of ACMD were designed and fabricated. The ACMDs consists an injection reservoir, a straight or serpentine channel, and a waste collection chamber. The width of the channel was 1mm with the depth being 100μm. Since the fabrication technologies have been discussed systematically in our previous works [26, 27], the fabrication process will only be briefly introduced as follows.

First, a 304 stainless steel film (100μm thick, Hongxing Company, China) was used for fabricating the mold. Five sheets of the stainless steel films were made into a stack and inserted between two clamping plates with its edge spot welded in case any vibration from the machining process can cause damage to the final surface quality. The straight and serpentine templates were patterned into the stainless steel films using wire electrical discharge machining (WEDM) (Fig. 2a). The detailed WEDM parameters can be found in Supplemental Information S1. Second, the hot embossing process was applied to transfer the mold patterns onto the excluded PMMA sheet (100mm long, 34mm wide and 1mm thick, Asahi, Kasei). From the bottom to the top, a polished stainless steel plate, the mold, the excluded PMMA sheet and another polished stainless plate were placed, respectively (Fig. 2b). The polished stainless plate (Haocheng

Corporation, China) was 600μm thick with its flatness of 0.012mm and average surface roughness Ra of 0.068μm. The detailed hot embossing parameters can be founded in Supplemental Information S2. Third, a CO_2 laser ablation system (JinBoshi, JBSCO2-50) scanned around the microchannel of the PMMA replica to generate a small bulge structure which we called laser-bulge (LB), with the laser power, scanning speed and the number of the passes of 14w, 5mm/s and 1 pass, respectively (Fig. 2c). The distance of between the LB and the microchannel was 500μm, which can be designed by the computer aided drawing program. The LB was used to concentrate the ultrasonic energy, which was prepared for the ultrasonic bonding process. Fourth, the PMMA replica was submitted to the CGUI treatment, with the treatment time of 5mins and another 5mins venting out the waste gas in the chamber (Fig. 2d). The distance between the PMMA replica and the UV lamp was set to be 5cm. It is important to note that the distance between the quartz plates and the modified surface can affect the resolution of the design significantly. When the distance was too large, the modification resolution of the design was decreased. That is probably because the UV irradiation, which transmitted though the different quartz plates, has interference with each other, resulting in some overlapping UV irradiation area on the surface. When the distance was too small, the resulting modification effectiveness was severely reduced. That may attributed to the fact that the amount of the O_3 molecules and the oxygen (O) atomic passing through the small gap was decreased and cannot fully react with the modification surface. After many experiments, it was found that the distance of 2-3mm was appropriate for the application. Finally, the ultrasonic bonding system (Dizo-ultrasonic NC-1800P) was applied to seal the cover and the PMMA replica, with the pressure of 0.25MPa and ultrasonic time of 0.6s (Fig. 2e).

3.4 Flow rate test

The flow rate test was carried out by using the ACMDs with the straight and serpentine microchannel and the 30μl deionized water mixed with red biological dyes (Ekear, C0154) was used as the experimental liquid. The flowing video was recorded using a digital camera (a6000, Sony Co., Japan), which is capable of providing a resolution of 1920×1080 pixels per frame at a frame rate of 50 frames/s (fps) and the software Corel VideoStudio X9 was used to analyse the flowing video. By tracing the flow meniscus, the average flow rate can be obtained by the flow path divided by the flow

time. To provide a control experiment, the flow rate tests for the ACMDs without modification and with conventional UV/ozone modification were also conducted.

3.5 A fully integrated POCT device for cTnI detection

POCT device. The CGUI method was applied in a fully integrated POCT device for the detection of cTnI. The POCT device was injection moulded with a 10:1(m/m) mixture of Poly (methyl methacrylate) and TiO_2 and featured an overall size of 100×20×4mm. Fig. 3a shows the design model of the POCT device as well as its functional components. The device integrates five functional areas including the whole blood filtering area, the sample introduction area, the comb-like delay/mixing area, the biosensing area and the waste reservoir area. In the whole blood filtering area, a membrane filter (Ahlstrom CytoSep, 1662) was utilized to extract the plasma from the whole blood. In the sample introduction area, the FITC labeled antibodies (FITC Ab.) were deposited, which can be washed off by the testing sample and flow into the next area. In the delay/mixing area, the flow direction changed into a zigzag one, making the FITC Ab. and the targeted antigen cTnI fully mixed and bound and more details about this comb-like structure can be found in our previous work [28]. The capture antibody (capture Ab.) in the biosensing area served to capture the targeted antigen. 150μl of the testing sample was injected into the device and the excessive sample flowed into the waste collection area, acting as a buffer to wash away the unbound reagents. Thus, by using this device, only one-step of sample injection operation is required before obtaining the testing results from a commercially available fluorescence detector (Finecare, FS-112). Mask A, C and E were arranged on different functional area of the device as shown in Fig. 3a. In this way, the selective wettability for the PMMA surface can be obtained, making the different functional area performing properly.

Antibody immobilization. A sandwich style immunoassay configuration was used to carry out the fluoroimmunoassay, where the FITC Ab. and capture Ab. were immobilized on the surface of the device, and then the targeted antigen solution washed off the FITC Ab. and bound to it, finally a remaining free epitope of the targeted antigen bound to the capture Ab. The testing result was determined by excitation and detection of the emitted

fluorescence from the FITC-labelled Ab., which is directly related to the concentration of captured antigens.

FITC labeled human specific monoclonal anti-cardiac cTnI detection antibodies, human specific monoclonal anti-cardiac cTnI capture antibodies, and human cTnI biomarkers used in this work were all provided by Wondfo Ltd. (Guangzhou, China). FITC Ab. and capture Ab. were diluted into 0.4mg/ml and 60μg/ml respectively with phosphate buffered saline (PBS, pH 7.4). 3μl of FITC Ab. solution was spotted onto the sample introduction area and 1μl capture Ab. solution was spotted onto the biosensing area using a non-contact spotter developed by our group (Fig. 3b). It has been reported previously that antibodies can be immobilized passively onto the PMMA surface by direct incubation [29]. It should be note that although some chemical modifications of the PMMA surface can improve antibody immobilization [30], such techniques however increase the complexity of the design and processing procedures and therefore a passive immobilization method was adopted in this work. During the spotting of antibody solutions, the temperature was fixed at 20^{o}C and the humidity was near the dew point to increase the evaporation time of the droplets. The substrate of the device was incubated at 30 ^{o}C for 3 hours subsequent to the spotting process and then it was sealed by the cover plate which was also made of PMMA using ultrasonic bonding method. The bonding process was illustrated in our previous work [31]. cTnI biomarker samples were prepared in PBS buffer and produced the concentrations of 50, 25, 10, 1, and 0.1 ng/ml for analysis. The minimum concentration of 0.1ng/ml was selected because it is within the range of clinically acceptable concentrations of cTnI biomarker (0.01–0.1 ng/ml) [23, 24] before the occurrence of an acute myocardial infarction.

4. Results and discussions

4.1 Effect of Cu film on UV transmittance

The sputtering time and the corresponding Cu thickness were listed in Table. 1. It should be noted that the mask A was not sputtered with Cu so that it can be used as a control group. The reasons of the Cu material being applied for the masks are as follows. First, the Cu material has strong adhesion strength on the quartz glass [20]. In our experiments, after at least 30 times UV irradiation modification, the modification effectiveness was not reduced, which indicated that

the adhesive strength between the Cu film and the quartz substrate was strong enough to ensure its long-term application. The second reason is that, compared with the other commonly-used materials in the lab such as Ag, Au, and Pt, Cu has the feature of being cost-effective.

Fig. 4a showed the effect of Cu film on UV transmittance with the emission wavelength ranging from 190nm to 400nm. It can be seen that with the increasing of the Cu thickness, the UV transmittance decreased accordingly. When the mask A was applied, which was not sputtered with Cu, the UV transmittance can be above 90%. When the mask F was used with the Cu thickness of 25nm, the UV light hardly transmitted through the mask with the UV transmittance less than 5%. Fig. 4b showed the UV transmittance when the wavelength was 190nm and 254nm, which was the emission wavelength of the UV lamp used in our experiments. It can be seen that the UV transmittance showed a gradient-variation following the different thickness of Cu film. Therefore, these masks can be used to adjust the UV irradiation and furthermore achieve the selective wettability modification purpose. Fig. 4c showed the picture of the CGUI device with the masks equipped. The transparency of the masks was different, which can be identified by the naked eyes. It is important to note that the size and the position of the masks can be easily changed using the device, which can achieve the flexible and selective function for different application demands.

4.2 Wettability of modified surface

The wettability of the modified PMMA surface was investigated through water contact angle (WCA) measurements with each measurement being repeated three times on three individual PMMA sheets. Fig. 5a showed the representative image of the WCA measurement results with the modification time of 5mins. Coupled with the results of the UV transmittance through different masks, it can be seen that the wettability of the modified area increased while the Cu film is decreasing. Thus, on one PMMA surface, five wettability-gradients were generated, which can make the WCA vary from 45.48^{o} to 77.41^{o}. Fig. 5b showed the relationship between the WCA and the modification time. It can be seen that without modification, the PMMA surface was nearly hydrophobic with a contact angle of 80.34 ± 2.56^{o}. The WCG decreased with the increasing of the modification time. When the modification time was 1min, the WCA of the area

beneath mask A was 66.71±3.55°. With the modification time increased to 9mins, the WCA of this area decreased to 29.18±2.35°. When the modification was longer than 9mins, the WCA almost remained the same. Nevertheless, due to the heat generated from the modification process, a small distortion can be found on PMMA sheet with the transparency also experiencing a slight decrease. Therefore, in this paper, the maximum modification time was set to be 9mins. It can also be seen from Fig. 5b that with mask A, the WCA decreased significantly following the increasing of the modification time. As the time increased from 1min to 9 mins, the WCA was decreased more than doubled. However, for the area with mask E, the variation of the WCA was not obvious. The WCA only decreased about 5° as the modification time increased from 1min to 9 mins. The reason for this phenomenon was probably due to the reason that as the thickness of the Cu on the mask increased, it became more difficult for the UV light to transmit through the mask, making the mask less sensitive to the UV irradiation. It resulted in the insensitivity of the modification time on the modification performance.

The stability of the CGUI performance has also been validated. The selective wettability of the PMMA surface can be maintained at least 60 days in air and Fig. 5c showed the variations of WCA of PMMA surfaces with aging time after 5 min modification. By taking the area with mask A as an example, the contact angle of this area was 47.03±1.77° right after the modification treatment, 47.16±2.35° after 1day, 49.27±3.11° after 5 days, 51.16±4.21° after 7 days, 54.07±3.87° after 14 days and 55.67±2.13° after 60 days. It can be seen that with aging time after 60 days, the WCA of the tested PMMA surface increased about 8°. Compared to the O_2- plasma treated surface, whose hydrophobic property can almost recover after several hours [15], the stability of the CGUI method has its advantage and can meet the demand for the majority of the microfluidic applications. It is important to note that the testing PMMA samples were stored in air. According to the prior report [32], if the samples are packed in either a dehumidified or vacuum environment, the long-term stability of UVO-treated plastics can last for up to 16 weeks.

4.3 ATR-FTIR and surface morphology investigation of the modified surface

ATR-FTIR. The chemical groups on the modified PMMA surfaces were characterized through ATR-FTIR. The spectra

were recorded from 4000 to 400 cm^{-1}. The UV/ozone-treated time for the PMMA surfaces was 5 mins. Fig. 6 showed the ATR-FTIR results of the modified surfaces using different masks. The absorption band at the wavenumber of 3000-3600 cm^{-1}, 2800-3000 cm^{-1}, 1600-1800 cm^{-1} and 1000-1300 cm^{-1} was assigned to stretching vibrations of O-H, C-H, C=O and C-O-C, respectively. It can be seen from Fig. 6 that after the modification, the intensity of the absorption band at the wavenumber of 3000-3600 cm^{-1} was increased, which indicated the generation of –OH group. Furthermore, while the masks A to E were applied, the intensity of the band at the wavenumber of 3000-3600 cm^{-1} decreased accordingly. This is because as the mask varied from A to E, the thickness of Cu film increased, which subsequently decreased the UV transmission through the mask. Thus, the intensity of the UV/ozone-induced functional groups was changed. To summarize this test, the UV/ozone can form the polar oxygen-containing functional group (–OH) on the PMMA surface, which can render the surface hydrophilic and the wettability of the surface can be adjusted by using different masks.

Surface morphology. The surface morphology of the modified surface was evaluated by using the white-light interferometer. The PMMA surface without modification was very smooth with the average surface roughness Ra of 1.032nm (Fig. 7f). After the UV/ozone treatment, the PMMA surface was significantly roughened in a nanoscale. A lot of nanoscale hillocks and pits were generated on the surface. With the mask changing from A to E, the height of these hillocks and pits decreased and their pitches and diameters increased, which can be observed in Fig. 7a ~ e. The formation of hillocks and pits was caused by UV-ozone induced polymer chain scission and local melting on the PMMA surface [33]. The masks can adjust the UV energy transmitted onto the surface. Therefore, it can provide a varying surface morphology for the surface. The relationship between the surface morphology and the wettability can be explained by Wenzel model [34]:

$$\cos\theta_w = r\cos\theta \tag{5}$$

where, r is the roughness factor. θ_w refers to the apparent contact angle of droplets on rough surfaces; θ is the eigen contact angle of droplets on smooth surfaces. The roughness factor r can be determined by the expression:

$$r = \frac{S_a}{S_p} \tag{6}$$

where, S_a refers to the solid–liquid actual contact area and S_b indicates the apparent contact area. The hillocks and pits can be taken as micropillars, then, the roughness factor can be expressed as:

$$r = [1 + \frac{4(h/d)}{(p/d)^2}] \tag{7}$$

Where, *h*, *d* and *p* refers to the height, diameter and pitch of the micropillars (Fig. 7g), respectively. Based on the above expressions, it can be seen that the wettability of the surface can be increased by increasing *h/d* or decreasing *p/d* of the micropillars, which is consistent with the phenomenon we observed in the experiment.

4.4 Capillary flow test in the ACDM

The capillary flow test was carried out with the characterization of the ACMD features being demonstrated in Supplemental Information S3. The capillary flow in the straight line microchannel was shown in fig. 8a ~ c. It can be seen from fig. 8a that without the modification of the microchannel, the flow meniscus only moved limited distance from the entrance. That is because the wettability of the microchannel was not sufficient to establish the capillary flow. As the device was treated by conventional UV/ozone method, the flow meniscus slowed down and almost stopped at the entrance of the waste collection chamber (fig. 8b). Furthermore, it can be seen that the liquid in the injection chamber was not fully pumped into the waste collection chamber, which can affect its application in some quantitative analysis. Fig. 8c showed the capillary flow in the ACDM modified by the CGUI method. It can be seen that by using different masks, different flow rate were generated, which varied from 215.4nl/s to 403.2 nl/s and 733.6 nl/s. The different flow rate can be applied for different applications, such as slow rate for incubation, medium rate for reaction and fast rate for waste washing. Moreover, the liquid in the injection chamber was emptied, which indicated that all the liquid in the injection chamber was driven into the waste collection chamber. From the capillary flow theory, it can be seen that the capillary flow rate is related to the capillary pressure difference which is inside and in front of the liquid. The capillary pressures inside and in front of the liquid are determined by the wettability and the geometry of the corresponding microchannel. For the conventionally UV modified microdevice, the wettability of the whole modified

surface had minimum variation. When the liquid reached the entrance of the waste collection chamber, the width of the microchannel increased, which resulted in the decreasing of the capillary pressure in front of the liquid. Thus, the capillary pressure difference decreased and the capillary flow slowed down and almost stopped. For the CGUI modified microdevice, since the UV transmittance of mask A was above 90%, the wettability of the waste collection chamber was almost the same with that of the no-mask area, which was higher than that of the preceding area. Therefore, although the geometry of the waste collection chamber was enlarged, the capillary pressure difference did not decrease severely and the liquid can rapidly fill the chamber. Fig. 8d ~ f showed the capillary flow in the serpentine microchannel. The flow behavior was similar as that in the straight line microchannel. The CGUI method can render the microchannel selective wettability, which resulted in the flow rate changing from 321.8nl/s to 543.7 nl/s and 817.3 nl/s.

4.5 Results for the detection of cTnI

In a typical ELISA assay, the reaction reagents are introduced sequentially, which means that each step requires manual operation. That has made the whole process highly labor-intensive especially when dealing with tens or hundreds of assays. Thanks to the large surface to volume ratios, the microfluidic system has the capability of simplifying the operation as well as reducing the reacting time to the order of minutes. However, most of the existing microfluidic platforms still involved at least two reagent input steps [7]. Or else, extra power supply such as centrifugal forces [35] or external pumps [36] was usually required. Here, we presented a one-step, fully integrated and capillary-driven microfluidic device for the detection of cTnI, which can be applied in the POCT area where people without medical background can easily perform the assay operation.

Fig. 9a showed the sample flow behavior in the POCT device. The operator only needs to inject 150μl testing sample into the device. Then, the membrane filter takes 15-20s to extract the plasma from the whole blood sample. Next, it flows into the sample introduction area and washes off the FITC Ab., which takes 10-15s. Subsequently, the sample solution takes about 2mins to pass through the delay/mixing area where the targeted antigen and FITC Ab. are mixed and bound. The capture Ab. in the biosensing area captures the bound antigen. The excessive sample solution acts as the

washing buffer, which first takes a rapid 15-20s to fill the waste reservoir Ⅰ and then takes another 160-180s to fill the waste reservoir Ⅱ, bringing the total assay duration to approximately 10mins. During the assay process, the flow rate of the sample solution is vital for the testing results. For example, the sample solution should flow fast enough to wash off the FITC Ab. in the sample introduction area. The flow rate in the delay/mixing area should be slow to provide enough time for the binding and mixing of the targeted antigen and FITC Ab. When it comes to the waste reservoir Ⅰ, a fast flow can rapidly remove the unbound reagents and decrease the background fluorescence. It can be seen that there were no complicated micropump or microvalve structures in the device and all the flow rate differences were generated by using the CGUI method. Mask A, C and E were arranged as shown in Fig. 9a. After 7mins of UV/ ozone treatment, the WCA of the modified surface was 39.37° (sample introduction area and waste reservoir area Ⅰ), 76.43° (delay/mixing area) and 56.14° (biosensing area and waste reservoir area Ⅱ). The reason why the FITC Ab. can be washed off and the capture Ab still remained on the substrate was attributed to the following two factors. Firstly, while the FITC Ab and capture Ab were both immobilized on the substrate, the immobilization strength of the FITC Ab was weaker than that of the capture Ab. That is because the surface wettability plays an important role in protein adsorption [37]. From the prior reports, it can be seen that in most cases more hydrophilic surfaces inhibits the absorption of proteins [38]. The WCA of the sample introduction area where the FITC Ab was immobilized was about 20^{o} lower than that of the biosensing area where the capture Ab was immobilized. The more hydrophilic surface decreased the immobilization strength of the FITC Ab. Then, the decreasing geometry and more hydrophilic property of the sample introduction area can provide stronger capillary pressure to wash off the FITC Ab. Fig. 9b showed the comparison of the detected fluorescence result by using the CGUI method and conventional UV/ozone modification as the cTnI concentration remained 10ng/ml. It can be seen that compared to the conventional UV/ozone modification, by using the CGUI method, the peak value of the fluorescence signal in the biosensing area enhanced by 52.4%, and the background fluorescence decreased by 43.7%. The reasons may be as follows. When the device was treated by 7mins conventional UV/ozone modification, the WCA of all the modified surface was about 38.79°. Under this condition, the comb-like

structure in the delay/mixing area cannot pinned the sample solution flow, which meant that the sample solution directly flowed over the area instead of the zigzag flow behavior as shown in Video S1. Thus, the FITC Ab. and the targeted antigen cannot be fully bound and mixed. Besides that the flow rate in the biosensing area was so fast that a lot of the bound antigen was washed away and cannot be capture by the capture Ab., resulting in the decrease of the fluorescence signal. On the other hand, as the sample solution reaches the entry of the waste reservoir, the microchannel was abruptly widened. Based on the theoretical analysis of capillary flow, the flow rate slowed down (Video S2) which caused the accumulation of the fluorescence particles, bringing about higher background fluorescence.

Fig. 9c depicted the average fluorescence detected from 5 repeat tests using independent devices for each concentration. A PBS solution with no biomarker was used as a control sample. It can be seen in Fig. 9c that the device performed efficiently within the examined range of cTnI, demonstrating good repeatability of the assay with cTnI spiked buffer samples. The lowest concentration detected using this device was 0.1ng/ml, which was clear above the blank sample intensity for the control samples. The lower detection limit (LDL) was calculated from the sum of the mean signal and 3 fold standard deviation (SD) obtained from the 15 fold blank sample measurements. The LDL was found to be approximately 85 pg/ml, which is well within the range of clinically acceptable cTnI detection concentrations (0.01–0.1 ng/ml), demonstrating its potential application in the POCT field. It should be noted that this device is still in the experimental stage. Although the whole blood has been used for the flow behavior test, the PBS-based solution was used to perform the cTnI detection. It can be anticipated that the LDL would be higher if the whole blood was used for the testing sample, since the additional biological components in the whole blood can affect the testing result and may bring about the cross reactivity issue. However, our intension in this paper is to generate the desired flow rate or wettability-gradient in the microchannel by using the CGUI method and demonstrate its potential application in the POCT area. This purpose has been clearly achieved in the current work. The clinical test of our device has been undergoing and we believe in the near future it can be a promising product in the POCT market.

Conclusions

In this paper, a controllable gradient UV irradiation (CGUI) method for PMMA surface was demonstrated. In this method, the quartz plates sputtered with different thickness of Cu were applied for the conventional UV/ozone modification to render the PMMA surface selective wettability. The WCA measurements showed that through 5mins treatment, the WCA of the PMMA surface can be varied from 45.48° to 77.41° continuously and can last up to 60 days. The quantity of the polar oxygen-containing functional group and the geometry of the nanoscale hillocks and pits structures generated by the UV/ozone treatment can be adjusted using different quartz plates, which led to the selective wettability performance. Different flow rate can be obtained in the autonomous capillary microfluidic device (ACMD), which can achieve the priming, time-delaying and emptying process automatically. By using this method, the lower detection limit of 85pg/ml for cTnI was obtained within 10mins. Compared with the conventional UV/ozone treatment, the fluorescence signal was enhanced by 52.4% and the background fluorescence decreased by 43.7%. In addition, this CGUI method should be applicable for some other polymers, such as polycarbonate (PC), polystyrene (PS), and cyclic olefin copolymer (COC), and also for some inorganic material, such as silicon.

Acknowledgements

This work was supported by the National Natural Science Foundation of China (51375076, 51475079), Science Fund for Creative Research Groups of NSFC (51621064) and the National Key Research & Development Plan (2016YFC1202503).This work was also supported by Fundamental Research Funds for the Central Universities (DUT15LAB12) and Natural Science Foundation of Liaoning Province (201602155).

References

[1] B. S. Hayes, A. N. Govyadinov, and P. E. Kornilovitch, Microfuidic switchboards with integrated inertial pumps, *Microfluid. Nanofluid.* 22 (2018) 15.

[2] L. Zhang, B. Jones, B. Majeed, Y. Nishiyama, Y. Okumura and T. Stakenborg, Study on stair-step liquid triggered capillary valve for microfluidic systems, *J. Micromech. Microeng.* 28 (2018) 065005.

[3] R. D. Chien R, Hot embossing of microfluidic platform, *Int. Commun. Heat Mass Transf.* 33 (2006) 645-653.

[4] K. Kistrup, C. E. Poulsen, P. F. Østergaard, K. B. Haugshøj, R. Taboryski, A. Wolff and M. F. Hansen, Fabrication and modelling of injection moulded all-polymer capillary microvalves for passive microfluidic control, *J. Micromech. Microeng.* 24 (2014) 125007.

[5] Y. Noma, K. Higashi, H. Aizawa, S. Kurosawa, H. Yatsuda, M. Nara and K. Terashima, Local surface modification of polymer material using low-temperature microplasma, *J. Photopolym. Sci. Tech.* 20 (2007) 785–792.

[6] H. Qi, T. Chen, L. Yao and T. Zuo, Hydrophilicity modification of poly(methyl methacrylate) by excimer laser ablation and irradiation, *Microfluid. Nanofluid.* 5 (2008) 139–143.

[7] M. I. Mohammed and M. P. Desmulliez, Autonomous capillary microfluidic system with embedded optics for improved troponin I cardiac biomarker detection, *Biosens. Bioelectron.* 61 (2014) 478–484.

[8] Y. Kwon, C. A. Hara, M. G. Knize, M. H. Hwang, K. S. Venkateswaran, E. K. Wheeler, P. M. Bell, R. F. Renzi, J. A. Fruetel and C. G. Bailey, Magnetic Bead Based Immunoassay for Autonomous Detection of Toxins, *Anal. Chem.* 80 (2008) 8416-8423.

[9] M. Yao, G. Shah and J. Fang, Highly Sensitive and Miniaturized Fluorescence Detection System with an Autonomous Capillary Fluid Manipulation Chip, *Micromachines* 3 (2012) 462-479.

[10] K. Tsougeni, D, Papageorgiou, A. Tserepi and E. Gogolides, "Smart" polymeric microfluidics fabricated by plasma processing: controlled wetting, capillary filling and hydrophobic valving, *Lab Chip* 10 (2010) 462-469.

[11] Y. Yamada, K. Takahashi, T. Ikuta, T. Nishiyama, Y. Takata, W. Ma and A. Takahara, Tuning Surface Wettability at the Submicron-Scale: Effect of Focused Ion Beam Irradiation on a Self-Assembled Monolayer, *J. Phys. Chem. C* 120 (2016) 274-280.

[12] V. D. Virgilio, S. Bermejo and L. Castañer, Wettability Increase by "Corona" Ionization, *Langmuir* 27 (2011) 9614–9620.

[13] J. Liu, T. Pan, A. T. Woolley and M. L. Lee, Surface-Modified Poly (methyl methacrylate) Capillary Electrophoresis Microchips for Protein and Peptide Analysis, *Anal. Chem.* 76 (2004) 6948-6955.

[14] J. H. Lee, S. K. Kim, H. H. Park and T. S. Kim, TiO_2 coated microfluidic devices for recoverable hydrophilic and hydrophobic patterns, *J. Micromech. Microeng.* 25 (2015) 035032.

[15] H. Shinohara, T. Kasahara, S. Shoji and J. Mizuno, Studies on low-temperature direct bonding of VUV/O3-, VUV- and O2 plasma-pre-treated poly-methylmethacrylate, *J. Micromech. Microeng.* 21 (2011) 085028.

[16] M. Zimmermann, H. Schmid, P. Hunziker and E. Delamarche, Capillary pumps for autonomous capillary systems, *Lab Chip* 7 (2007) 119–125.

[17] M. Zimmermann, P. Hunziker and E. Delamarche, Valves for autonomous capillary systems, *Microfluid. Nanofluid.* 5 (2008) 395-402.

[18] D. A. Bolon and C. O. Kunz, Ultraviolet depolymerization of photoresist polymers, *Polym. Eng. Sci.* 12 (1972) 109-111.

[19] C. W. Tsao, L. Hromada, J. Liu, P. Kumar and D. L. DeVoe, Low temperature bonding of PMMA and COC microfluidic substrates using UV/ozone surface treatment, *Lab Chip* 7 (2007) 499–505.

[20] J. Liu, L. He, L. Wang, Y. Man, L. Huang, Z. Xu, D. Ge, J. Liu, C. Liu and L. Wang, Significant Enhancement of the Adhesion between Metal Films and Polymer Substrates by UV–Ozone Surface Modification in Nanoscale, *ACS Appl. Mater. Interfaces* 8 (2016) 30576-30582.

[21] H. Wei and G. J. Su, Using Hydrophilic Effect to Fabricate Self-Assembled Microlens Array by UV/Ozone Modification, *IEEE Photonics Technol. Lett.* 24 (2012) 300-302.

[22] S. Almohammed, S. O. Oladapo, K. Ryan, A. L. Kholkin, J. H. Rice and B. J. Rodriguez, Wettability gradient-induced alignment of peptide nanotubes as templates for biosensing applications, *Rsc. Adv.* 6 (2016) 41809-41815.

[23] D. A. Morrow, C. P. Cannon, R. L. Jesse, L. K. Newby, J. Ravkilde, A. B. Storrow, A. H. B. Wu and R. H. Christenson, National Academy of Clinical Biochemistry Laboratory Medicine Practice Guidelines: Clinical characteristics and utilization of biochemical markers in acute coronary syndromes, *Clin. Chem.* 53 (2007) 552–574.

[24] B. McDonnell, S. Hearty, P. Leonarda and R. O'Kennedy, Cardiac biomarkers and the case for point-of-care testing, *Clin. Biochem.* 42 (2009) 549–561.

[25] J. M. Chen, P. C. Huang and M. G. Lin, Analysis and experiment of capillary valves for microfluidics on a rotating disk, *Microfluid. Nanofluid.* 4 (2008) 427-437.

[26] C. Liang , C. Liu , Z. Liu , F. Meng and J. Li, Laser-bulge based ultrasonic bonding method for fabricating multilayer thermoplastic microfluidic devices, *J. Micromech. Microeng.* 27 (2017) 115012.

[27] C. Liang , F. Meng, J. Li and C. Liu, Using CO2-laser bugle for ultrasonic bonding of thermoplastic microfluidic devices, *J. Mater. Process. Technol.* 252 (2018) 25–33.

[28] J. Li, C. Liang , B. Zhang and C. Liu, A comblike time-valve used in capillary-driven microfluidic devices, *Microelectron. Eng.* 173 (2017) 48–53.

[29] M. I. Mohammed and M. P. Desmulliez, Planar lens integrated capillary action microfluidic immunoassay device for the optical detection of troponin I, *Biomicrofluidic* 7 (2013) 064112.

[30] S. Wang, M. Esfahani, U. A. Gurkan, F. Inci, D. R. Kuritzkes and U. Demirci, Efficient on-chip isolation of HIV subtypes, *Lab Chip* 12 (2012) 1508–1515.

[31] J. Li, F. Meng, C. Liang and C. Liu, Energy director structure and self-balancing jig for the ultrasonic bonding of microfluidic chips, *Micro Nano Lett.* 12 (2017) 453–457.

[32] T. Y. Lin, T. T. Pfeiffer, and P. B. Lillehoj, Stability of UV/ozone-treated thermoplastics under different storage conditions for microfluidic analytical devices, *RSC Adv.* 7 (2017) 37374.

[33] A. Bhattacharyya and C. M. Klapperich, Mechanical and chemical analysis of plasma and ultraviolet–ozone surface treatments for thermal bonding of polymeric microfluidic devices, *Lab Chip* 7 (2007) 876–882.

[34] R. N. Wenzel, Resistance of solid surfaces to wetting by water, *Ind. Eng. Chem.* 8 (1936) 988–994.

[35] S. Lutz, E. Lopez-Calle, P. Espindola, C. Boehm, T. Brueckner, J. Spinke, M. Marcinowski, T. Keller, A. Tgetgel, N. Herbert, T. Fischer and E. Beiersdorf, A fully integrated microfluidic platform for highly sensitive analysis of immunochemical parameters, *Analyst* 142 (2017) 4206–4214.

[36] B. Mosadegh, T. Bersano-Begey, J. Y. Park, M. A. Burns and S. Takayama, Next-generation integrated microfluidic circuits, *Lab Chip* 11 (2011) 2813–2818.

[37] J. D. Andrade, and V. Hlady, Protein adsorption and materials biocompatibility: a tutorial review and suggested hypotheses, *Adv. Polymer Sci.,* 79 (1986) 1-63.

[38] M. Rabe, D. Verdes, and S. Seeger, Understanding protein adsorption phenomena at solid surfaces, *Adv. Colloid Interface Sci.,* 162 (2011) 87–106.

Author Biographies:

Liang Chao is a PhD student at Dalian University of Technology. He received his master's degree in mechanical engineering from Dalian Jiaotong University in 2014. He is the author or coauthor of 9 papers in SCI-indexed journals and 8 patents. His works focus on the design and fabrication of microfluidic devices.

Yuanchang Liu is a lecturer at University College London. He received his PhD in mechanical engineering from University College London in 2016. His research interests include MEMS and microfluidics.

Liu Chong is a professor in the School of Mechanical Engineering, Dalian University of Technology, China. He received his PhD from Huazhong University of Science and Technology (China) in 1993. He is the vice director of the MNST and the leader of the Microfluidics Group at MNST. He is the author or coauthor of more than 50 papers in SCI-indexed journals, 16 patents, and 2 books. He is interested in microfluidics and micro- and nanotechnology.

Li Xia is a master's student at Dalian University of Technology. She received her bachelor's degree in mechanical engineering from Qingdao Technology University in 2015. Her work focuses on the microfluidics and surface modification of materials.

Li Chen is an engineer in the key Laboratory for Micro/Nano Technology, Dalian University of Technology, China. She received her master's degree in mechanical engineering from Dalian University of Technology. Her researches focus on the test and characterization of microfluidic devices.

Chunzheng Duan is an associate professor in the School of Mechanical Engineering, Dalian University of Technology, China. He received his PhD from Dalian University of Technology. His work focuses on the design and microfabrication of mold for microfluidic devices.

Li Jingmin is a professor at Dalian University of Technology. He received his PhD in mechanical engineering from Dalian University of Technology in 2010. He is the author of more than 20 journal papers in SCI-indexed journals, 25 patents, and 2 books. His recent works focus on MEMS, microfluidics, and biomimics.

Figure captains

Fig.1 Schematic diagram of CGUI method and its device. (a) Illustration of the CGUI method. (b) Solid design model of the CGUI device.

Fig.2 Schematic diagram of the whole fabrication process. (a) Mold fabrication via WEDM. (b) Hot embossing. (c) Generation of the LB. (d) CGUI modification process. (e) Ultrasonic bonding process.

Fig.3 Schematic diagram for cTnI detecion. (a) The fully integrated POCT device and its functional components. (b) A non-contact spotter for the antibody spotting process. Note: Ab. is the abbreviation of antibody.

Fig.4 Effect of Cu film on UV transmittance. (a) Effect of Cu film on UV transmittance with the emission wavelength ranging from 190nm to 400nm. (b) The UV transmittance at the emission wavelength of 190nm and 254nm. (c) Picture of CGUI device and the inserted masks. Insert ⅰ)：mask B with the Cu film thickness of about 7nm and the UV transmittance of about 60%. Insert ⅱ)：mask C with the Cu film thickness of about 11nm and the UV transmittance of about 40%. Insert ⅲ)：mask D with the Cu film thickness of about 14nm and the UV transmittance of about 30%. Insert ⅳ)：mask E with the Cu film thickness of about 19nm and the UV transmittance of about 10%.

Fig.5 Water contact angle (WCA) measurements of the modified PMMA surfaces. (a) Representative images of WCA measurement results for the PMMA surface with the modification time of 5mins. (b) WCA measurement results for the modified PMMA surface at different modification time. (c) Variations of WCA of PMMA surfaces with aging time after 5 min modification.

Fig.6 ATR-FTIR results of the surfaces using different masks. Insert: absorption band at the wavenumber of 3000-4000 cm^{-1}.

Fig.7 Surface morphology investigation of the modified surface. Surface morphology by using different masks: (a) with mask A. (b) with mask B. (c) with mask C. (d) with mask D. (e) with mask E. (f) without modification. (g) The schematic diagram of Wenzel state.

Fig.8 Capillary flow pictures in the ACMD. (a) Straight microchannel without modification. (b) Straight microchannel with conventional UV/ozone modification. (c) Straight microchannel with CGUI modification. (d) Serpentine microchannel without modification. (e) Serpentine microchannel with conventional UV/ozone modification. (f) Serpentine microchannel with CGUI modification. The capital letters in the graph indicates the mask code.

Fig.9 Results for the detection of cTnI. (a) Sample flow behavior in the POCT device. The scale bar indicates 1mm. (b) Comparison of the detected fluorescence result by using the CGUI method and conventional UV/ozone modification. (c) Detected fluorescence for various concentrations of cTnI samples. The solid line is a guide to the eyes.

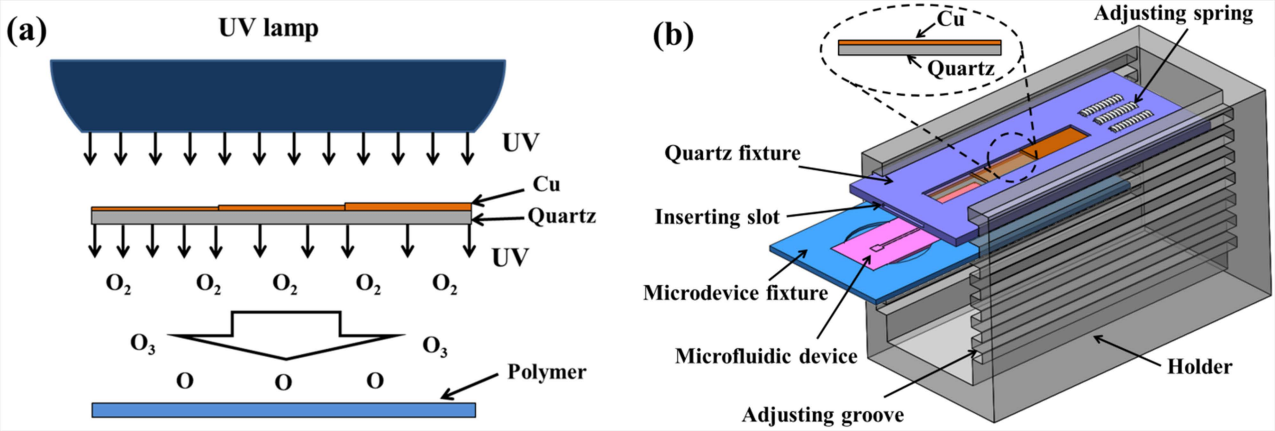
(a)
UV lamp
UV
Cu
Quartz
UV
O2
O2
O2
O2
O2
O3
O3
O
O
O
Polymer
(b)
Cu
Quartz
Adjusting spring
Quartz fixture
Inserting slot
Microdevice fixture
Microfluidic device
Holder
Adjusting groove

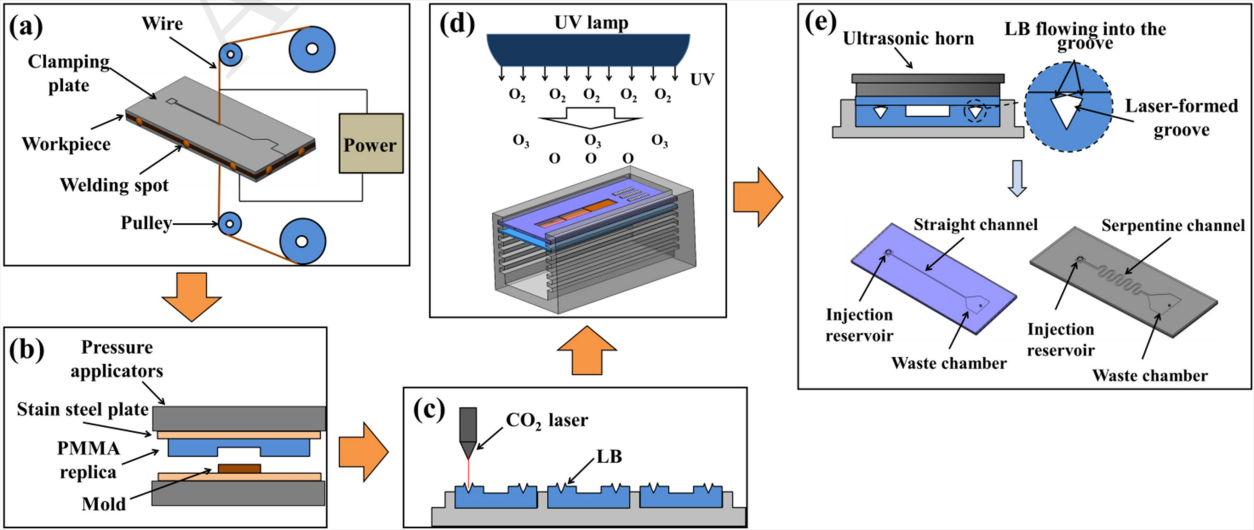
(a)
Wire
Clamping plate
Workpiece
Welding spot
Pulley
Power
(b)
Pressure applicators
Stain steel plate
PMMA replica
Mold
(c)
CO_2 laser
LB
(d)
UV lamp
UV
O_2 O_2 O_2 O_2 O_2
O_3 O_3 O_3
O O O
(e)
Ultrasonic horn
LB flowing into the groove
Laser-formed groove
Straight channel
Serpentine channel
Injection reservoir
Waste chamber
Injection reservoir
Waste chamber

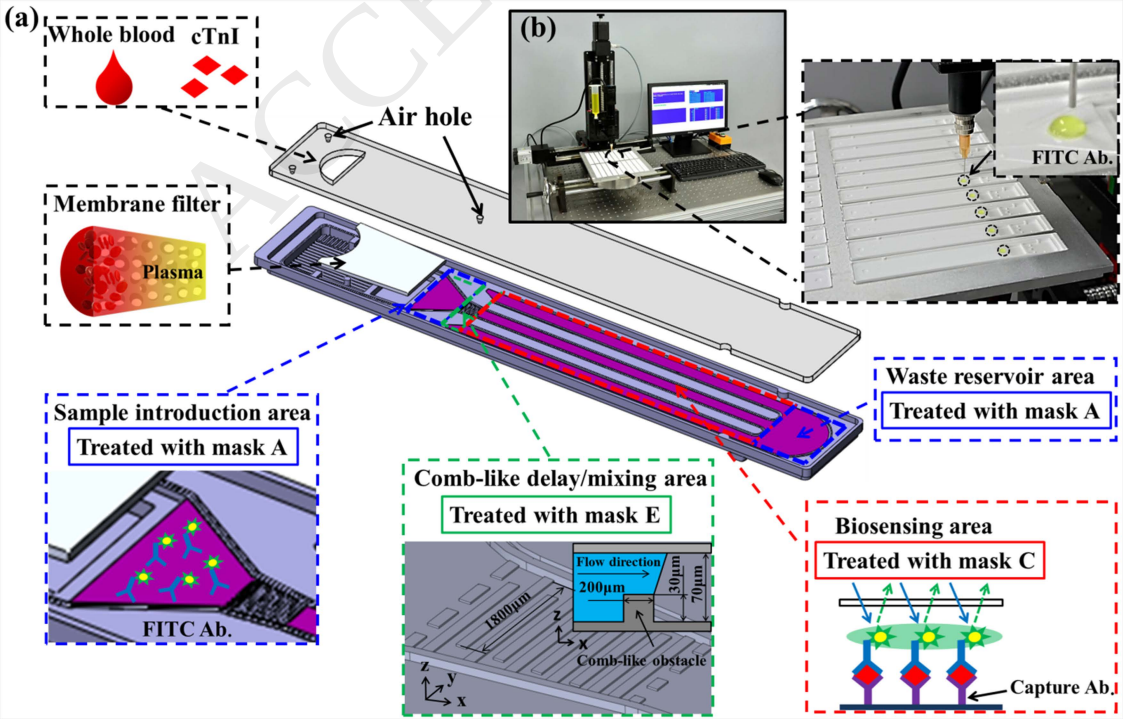
(a)
Whole blood
cTnI
Air hole
(b)
FITC Ab.
Membrane filter
Plasma
Waste reservoir area
Treated with mask A
Sample introduction area
Treated with mask A
FITC Ab.
Comb-like delay/mixing area
Treated with mask E
Flow direction
200μm
30μm
70μm
1800μm
Comb-like obstacle
Biosensing area
Treated with mask C
Capture Ab.

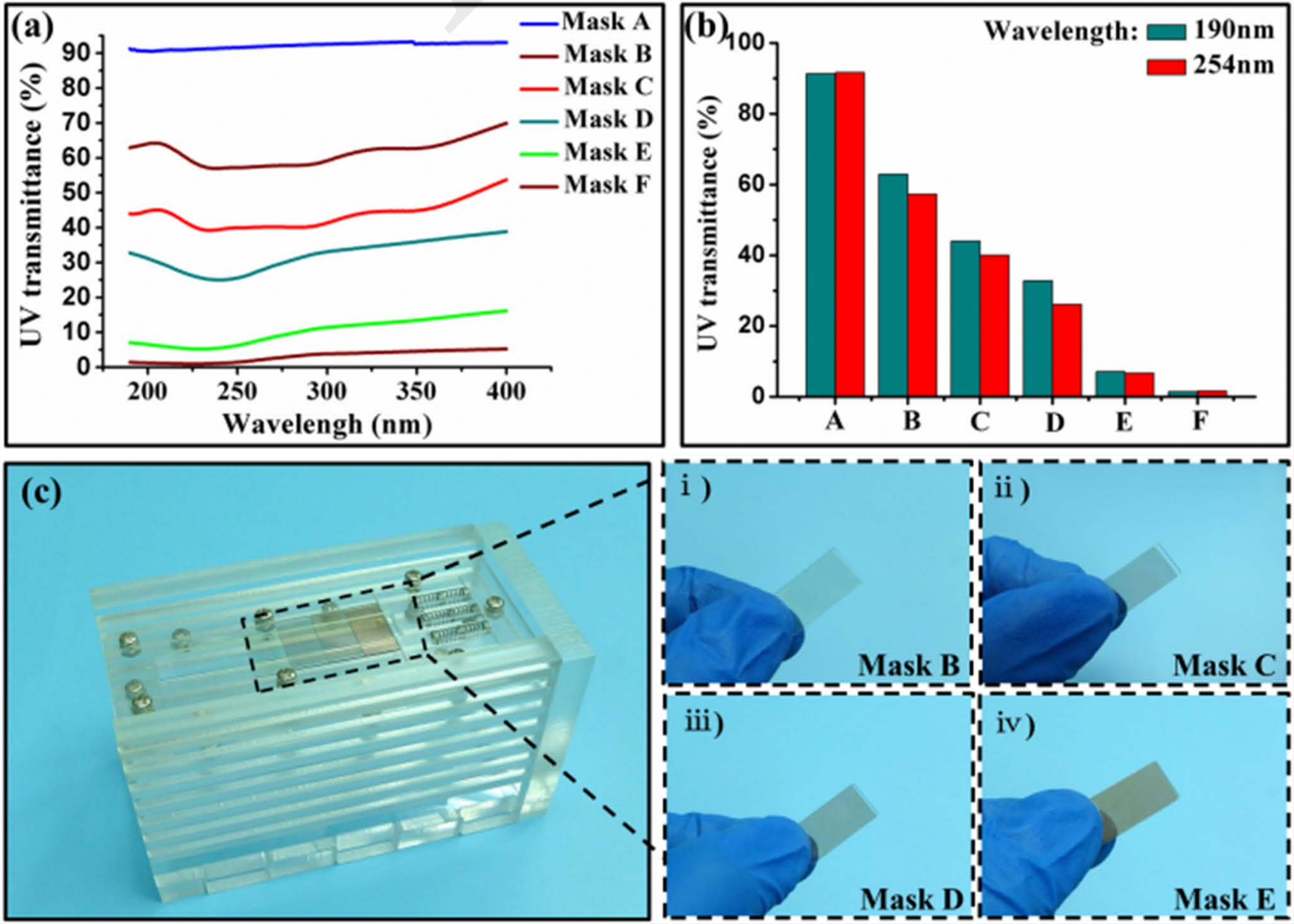
(a)
UV transmittance (%)
Wavelengh (nm)
Mask A
Mask B
Mask C
Mask D
Mask E
Mask F
(b)
UV transmittance (%)
Wavelength:
190nm
254nm
A
B
C
D
E
F
(c)
i)
Mask B
ii)
Mask C
iii)
Mask D
iv)
Mask E

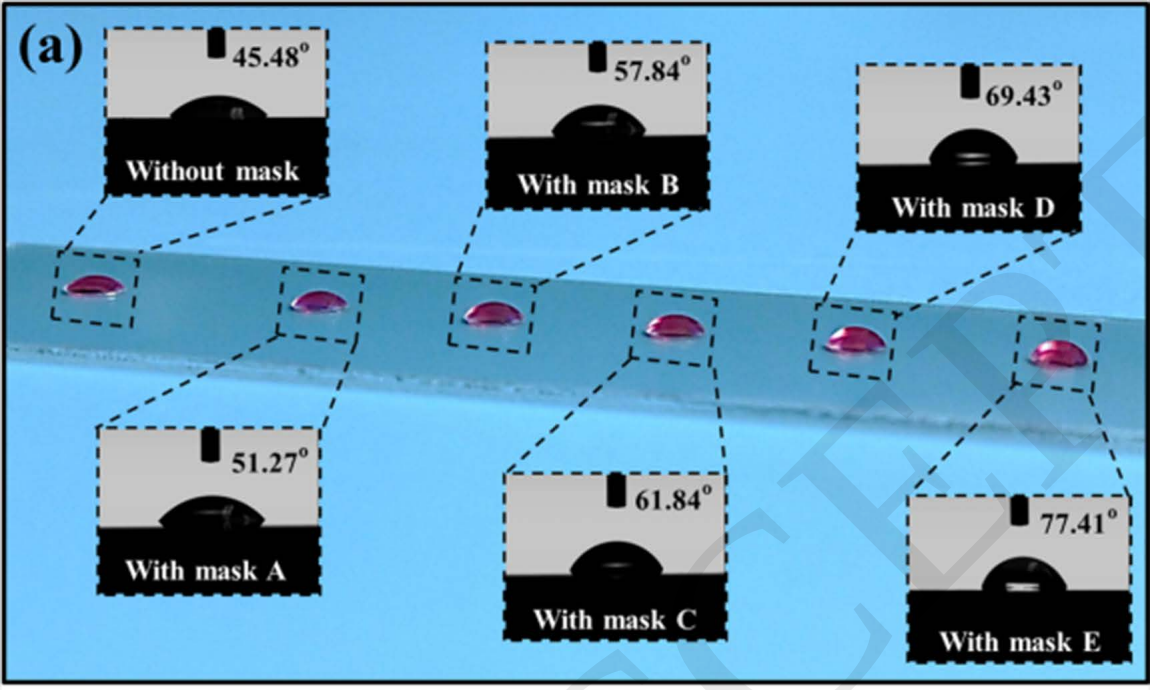
(a)
45.48°
Without mask
57.84°
With mask B
69.43°
With mask D
51.27°
With mask A
61.84°
With mask C
77.41°
With mask E

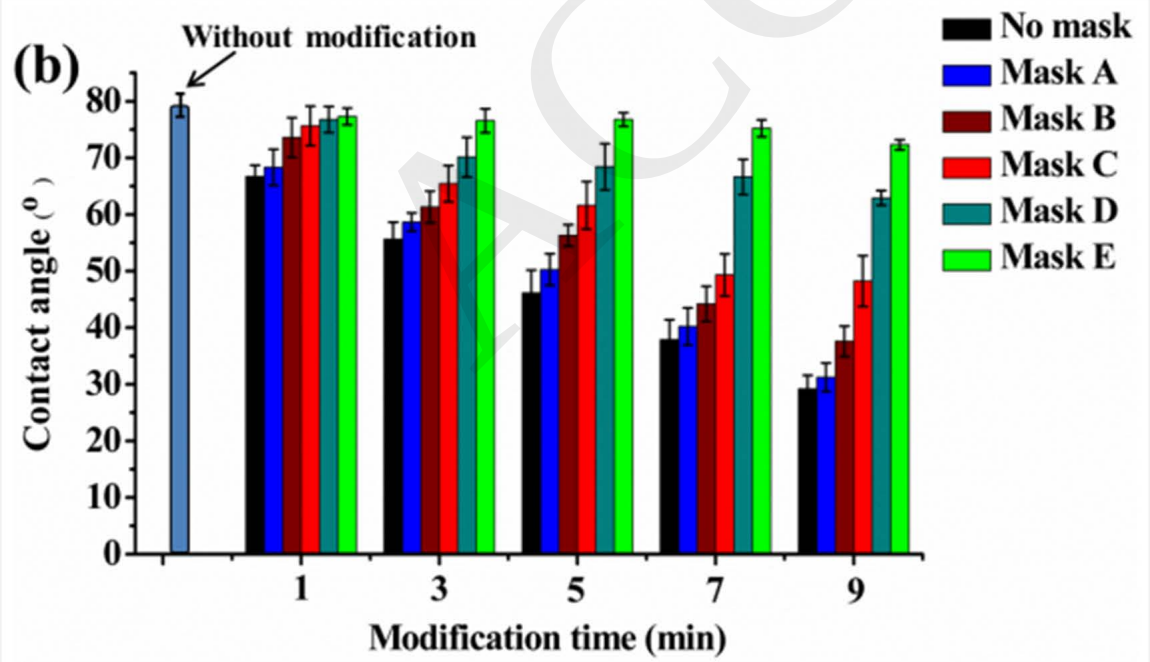
(b)
Without modification
No mask
Mask A
Mask B
Mask C
Mask D
Mask E
Contact angle (°)
0
10
20
30
40
50
60
70
80
1
3
5
7
9
Modification time (min)

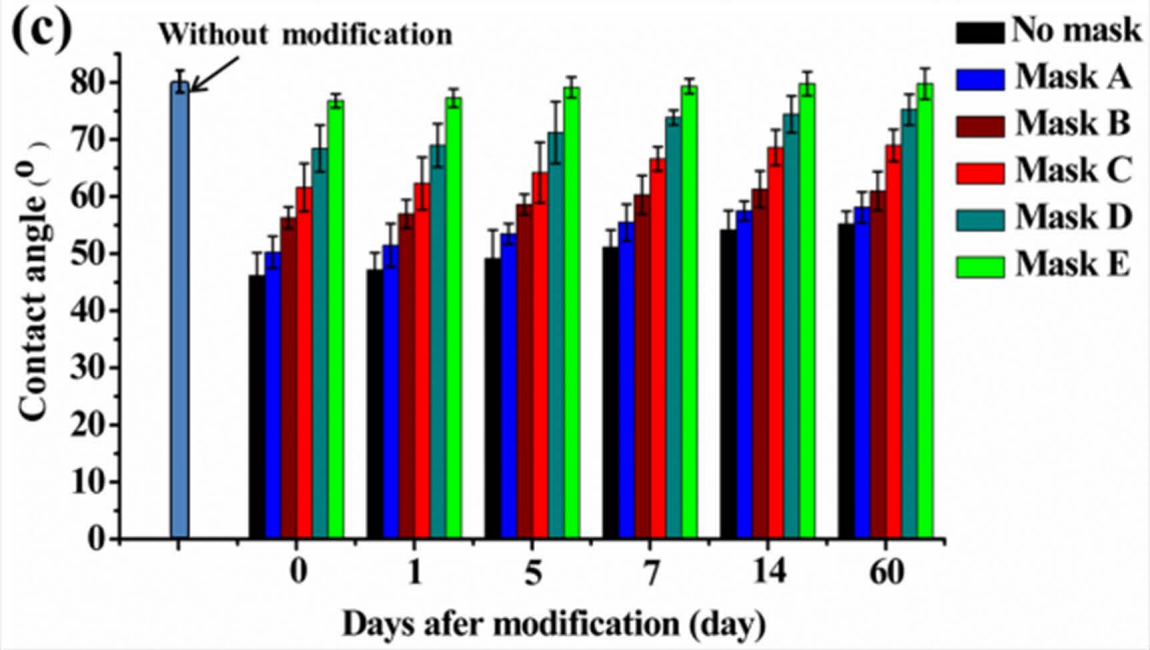
(c)
Without modification
No mask
Mask A
Mask B
Mask C
Mask D
Mask E
Contact angle (°)
0
10
20
30
40
50
60
70
80
0
1
5
7
14
60
Days afer modification (day)

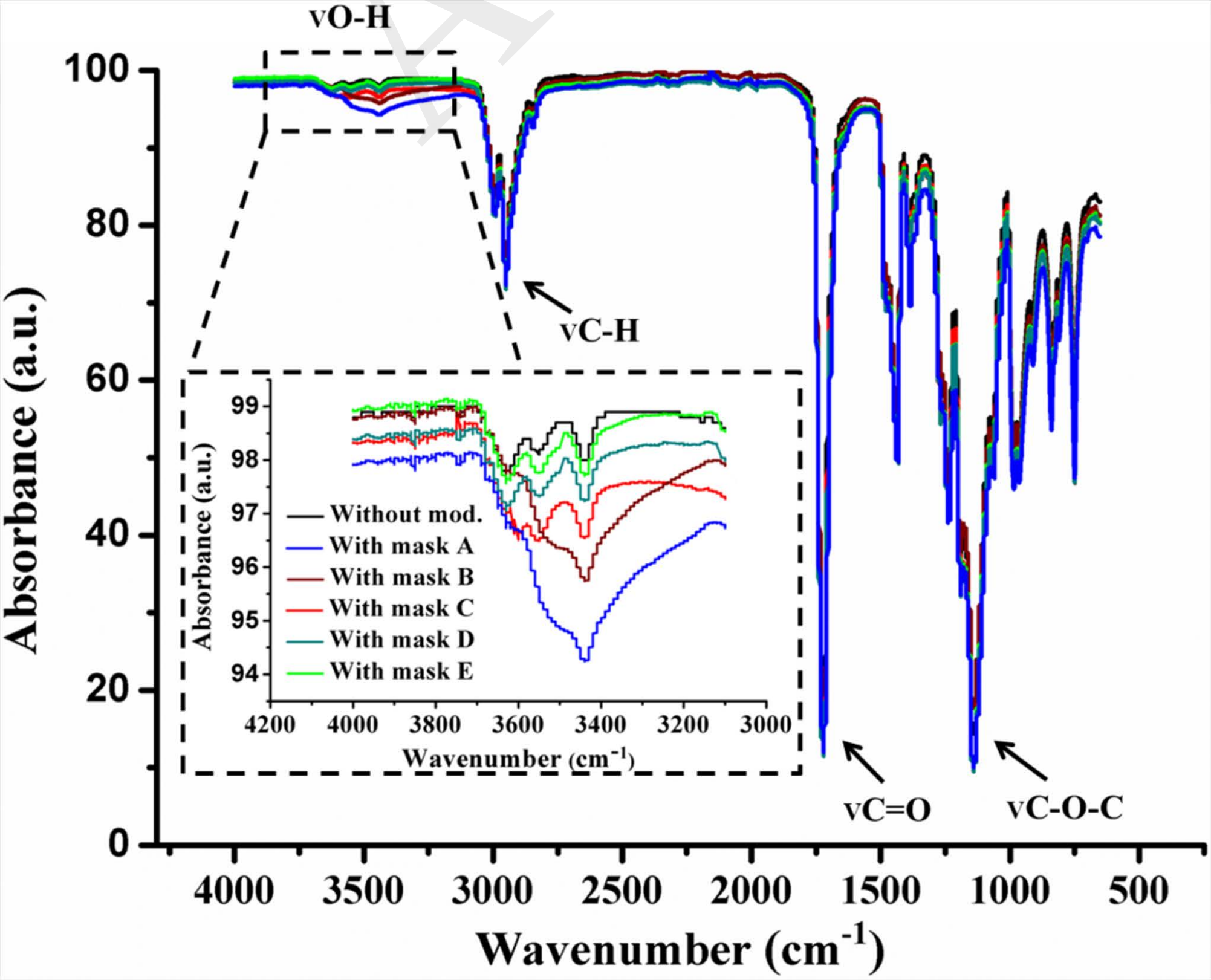
vO-H
vC-H
vC=O
vC-O-C
Absorbance (a.u.)
Wavenumber (cm-1)
100
80
60
40
20
0
4000
3500
3000
2500
2000
1500
1000
500
Absorbance (a.u.)
99
98
97
96
95
94
Without mod.
With mask A
With mask B
With mask C
With mask D
With mask E
4200
4000
3800
3600
3400
3200
3000
Wavenumber (cm-1)

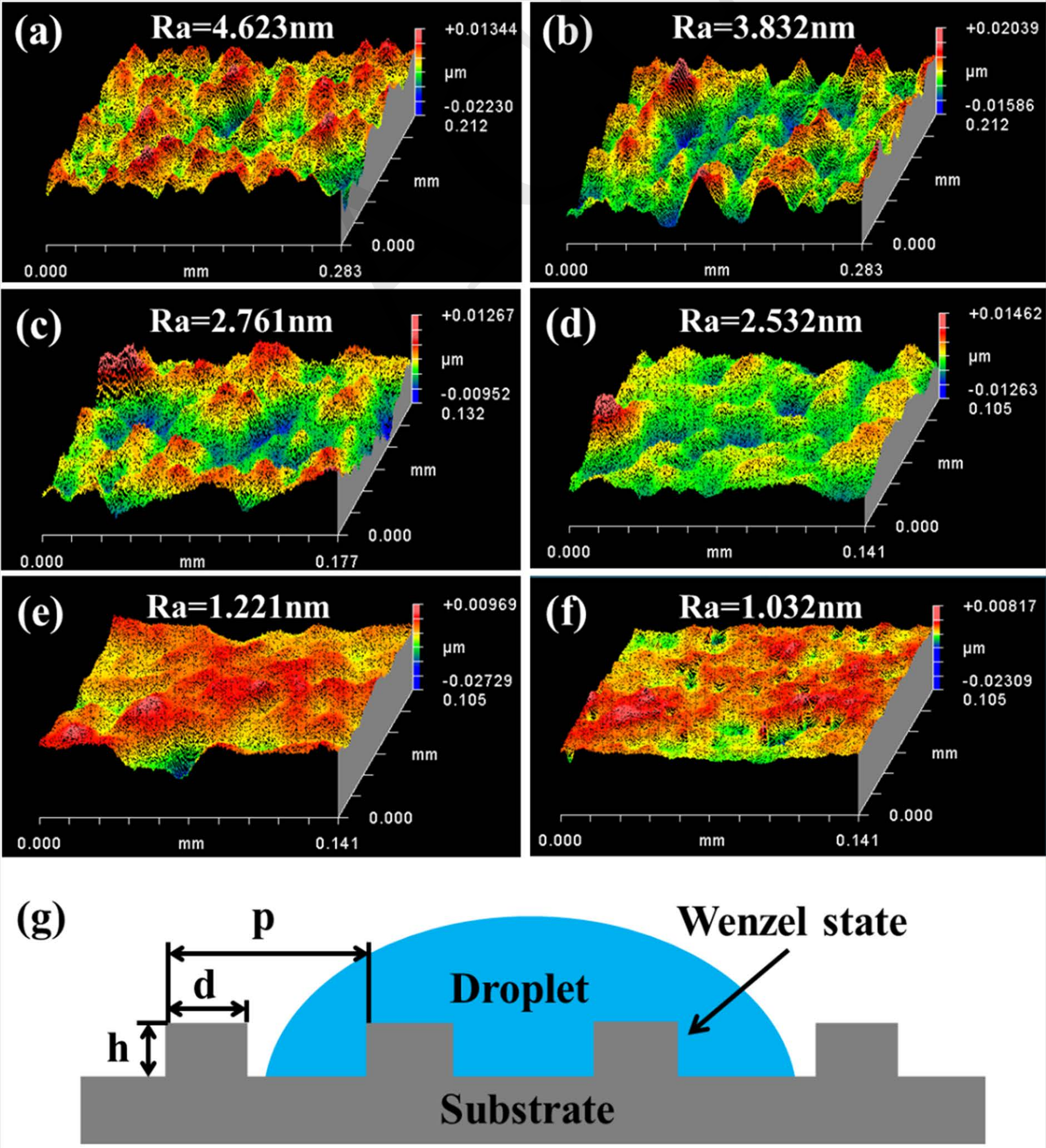
(a)
Ra=4.623nm
+0.01344
μm
-0.02230
0.212
mm
0.000
0.000
mm
0.283
(b)
Ra=3.832nm
+0.02039
μm
-0.01586
0.212
mm
0.000
0.000
mm
0.283
(c)
Ra=2.761nm
+0.01267
μm
-0.00952
0.132
mm
0.000
0.000
mm
0.177
(d)
Ra=2.532nm
+0.01462
μm
-0.01263
0.105
mm
0.000
0.000
mm
0.141
(e)
Ra=1.221nm
+0.00969
μm
-0.02729
0.105
mm
0.000
0.000
mm
0.141
(f)
Ra=1.032nm
+0.00817
μm
-0.02309
0.105
mm
0.000
0.000
mm
0.141
(g)
p
d
h
Droplet
Wenzel state
Substrate

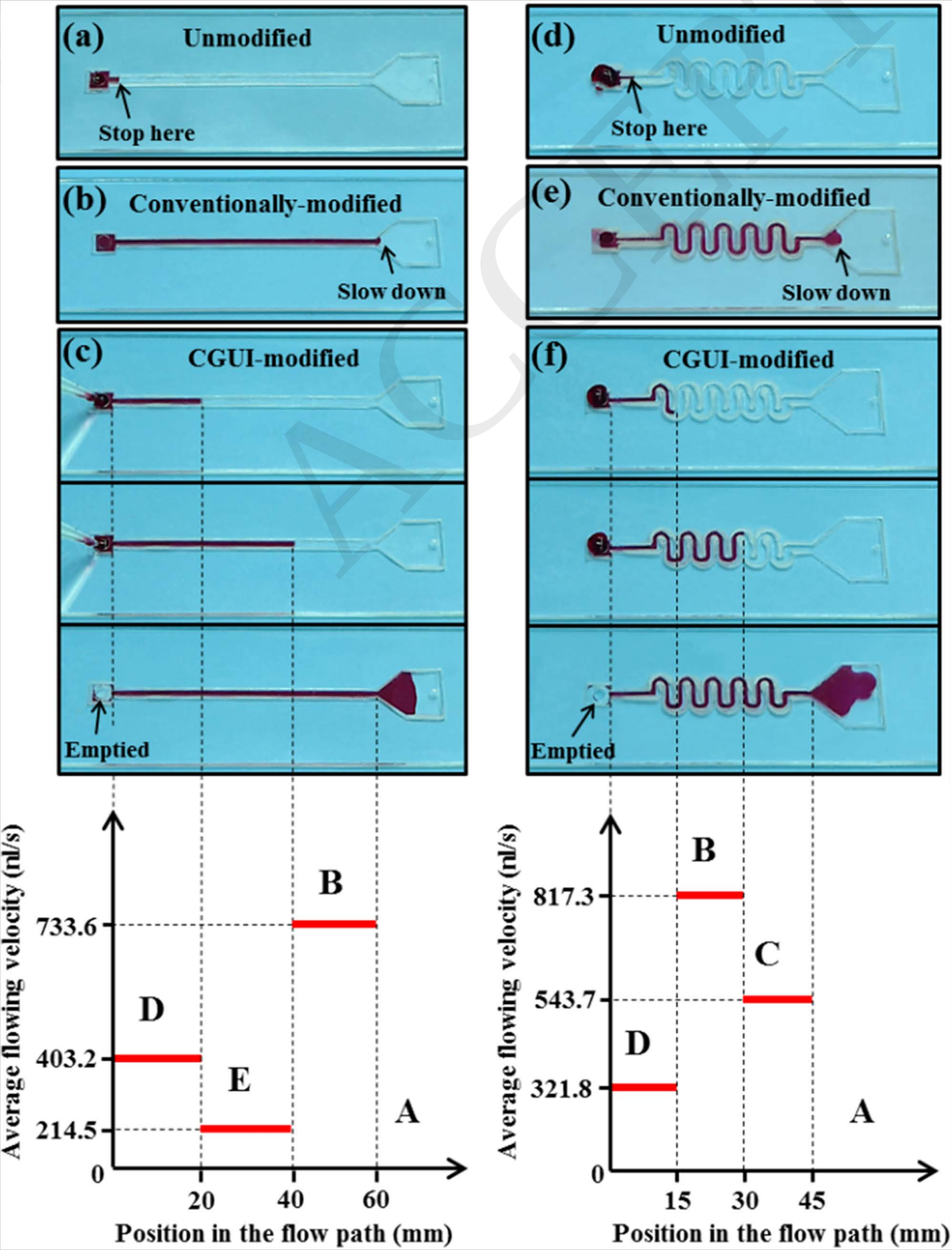
(a) Unmodified
Stop here
(b) Conventionally-modified
Slow down
(c) CGUI-modified
Emptied
(d) Unmodified
Stop here
(e) Conventionally-modified
Slow down
(f) CGUI-modified
Emptied
Average flowing velocity (nl/s)
733.6
403.2
214.5
0
B
D
E
A
20
40
60
Position in the flow path (mm)
Average flowing velocity (nl/s)
817.3
543.7
321.8
0
B
C
D
A
15
30
45
Position in the flow path (mm)

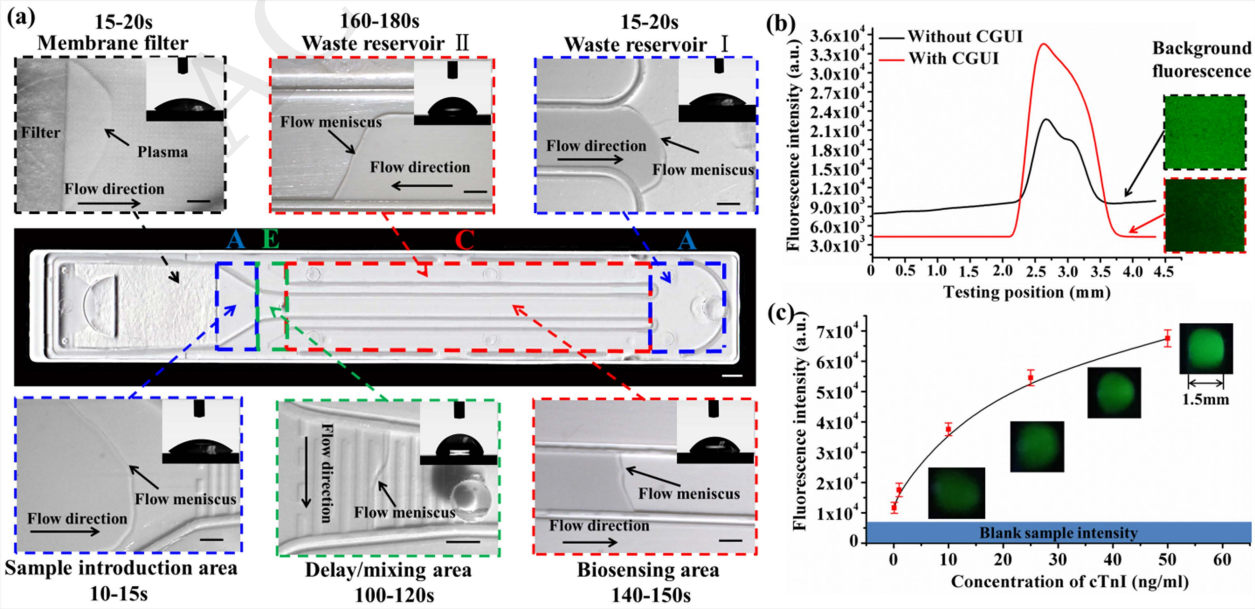
(a)
15-20s
Membrane filter
Filter
Plasma
Flow direction
160-180s
Waste reservoir Ⅱ
Flow meniscus
Flow direction
15-20s
Waste reservoir Ⅰ
Flow direction
Flow meniscus
A
E
C
A
Flow direction
Flow meniscus
Sample introduction area
10-15s
Flow direction
Flow meniscus
Delay/mixing area
100-120s
Flow meniscus
Flow direction
Biosensing area
140-150s
(b)
Without CGUI
With CGUI
Background fluorescence
Fluorescence intensity (a.u.)
Testing position (mm)
(c)
Fluorescence intensity (a.u.)
1.5mm
Blank sample intensity
Concentration of cTnI (ng/ml)

Table 1 The sputtering time and Cu thickness of the masks.

	Mask A	Mask B	Mask C	Mask D	Mask E	Mask F
Sputtering time (s)	_	2	5	8	11	14
Cu thickness (nm)	_	7	11	14	19	25